Comparison of RC-model and FEM-model for a PCM-plate storage including free convection

Hannah Neumann, Sebastian Gamisch, Stefan Gschwander*

Fraunhofer Institute for Solar Energy Systems ISE, Freiburg
*Corresponding author: tel: +49 761 4588-5494 | fax: +49 761 4588 9000 | stefan.gschwander@ise.fraunhofer.de

Highlights

- Latent heat storage based on FracTherm®-plates using D-mannitol as PCM
- Development of simplified RC-model including free convection during PCM melting
- Comparison of simplified RC-model to numerical FEM-model
- Validation of FEM-model with experimental data
- Deviation of outlet fluid temperature of RC-model and FEM-model of 0.62 K

Abstract

Latent heat storage is one option to increase the efficiency and reduce CO_2-emissions of process heat applications in the temperature range between 100 °C and 250 °C. In the present study a latent heat storage system based on flown through heat exchanger plates according to the FracTherm®-design is examined. The sugar alcohol D-mannitol is used as PCM. A simplified capacity resistor (RC) simulation model is developed. In contrast to common RC-models, this model can simulate free convection of the storage material in liquid phase during charging. Additionally, a detailed physical simulation model based on the Finite-Element-Method is developed and validated with measured data. A verification of the new RC-model and the FEM-model is carried out. The mean deviation of the outlet fluid temperature between both models is 0.62 K. The mean deviation of the PCM-temperature is 0.85 K. Due to the 20 to 30 times shorter simulation time, the RC-model is well suited for dimensioning and optimizing plate type heat exchangers for latent heat storages.

Keywords

Phase change material, D-mannitol, FracTherm®, RC-model, FEM-model, free convection

Graphical abstract

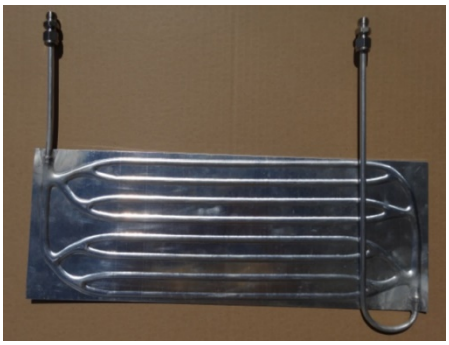

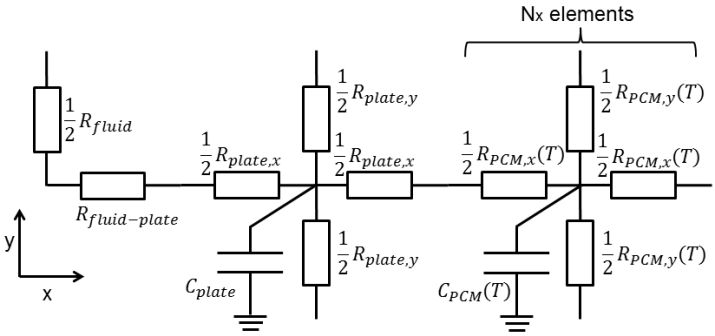

Nomenclature

Symbols

$\dot{Q}$	W	Heat flow
c_p	J/(kg K)	Specific heat capacity
$\dot{m}$	kg/s	Mass flow
$\dot{q}$	W/m^2	Heat flux
$\dot{q}$	W/m^3	Volumetric heat flux
h	J/kg	Specific Enthalpy
A	m^2	Area
A	1	Aspect ratio
C	J/K	Heat capacity
D	K	Mean deviation
F	N, N/m^3	Force
H	m	Height
R	K/W, Ω	Resistance
Ra	1	Rayleigh-Number
T	K	Temperature
V	m^3	Volume
b	m	width
d	m	Thickness
f	1	Fraction
g	m/s^2	Gravitational constant
l	m	Length
m	kg	Mass
n	1	Number
p	Pa	Pressure
t	s	Time

v	m/s	Velocity
α	W/(m^2 K)	Heat transfer coefficient
β	1/m	Volumetric expansion coefficient
η	Pa s	Dynamic Viscosity
λ	W/(m K)	Heat Conductivity
ρ	kg/m^3	Density
ϵ	1	convective enhancement factor

Abbreviations

1D	one-dimensional
2D	two-dimensional
3D	three-dimensional
CFD	Computational Fluid Dynamics
DSC	Differential Scanning Calorimeter
FEM	Finite-Element-Method
KNO_3	Potassium nitrate
$NaNO_3$	Sodium nitrate
PCM	Phase Change Material
PTFE	Polytetrafluoroethylene
RC	Resistance Capacity

Subscripts

Cond	Conduction
Conv	Convection
crit	critical
FEM	Finite-Element-Method
in	Inlet
l	Liquid
m	Melt
meas	Measurement
out	outlet
PCM	Phase Change Material
s	Solid
sim	Simulation
tot	Total

1 Introduction

One of the major challenges nowadays is the reduction of worldwide greenhouse gas emissions, thereby faciliatating the protection of the climate. One measure to reach this goal is to reduce and make full use of waste heat. In industrial processes, the utilization of thermal storage can, for example, contribute to the peak-load shifting [1, S. 4], and consequently reduce the generation of waste heat.

In process heat applications, defined in the temperature range between 100 °C and 250 °C [2, S. 536], water can only be used as pressurised heat storage medium. These storages are expensive because the vessels are required to tolerate high pressure [3, S. 48]. Alternative pressureless heat storages use, for example, thermal oil, rocks, concrete or ceramics as storage material. However, these materials have a low specific heat capacity, and thus big storage volumes are needed, given a small temperature application range.

For applications which require high heat capacity and small temperature application ranges, latent heat storage is an attractive alternative. The latent heat storage tends to be achieved using the so-called Phase Change Materials (PCM) as storage media, due to their high thermal energy storage density within an almost constant temperature.

Process heat storages are usually short term storages (i.e. storages that lasts for between hours and days) and tend to deliver higher power [2, S. 536]. In addition, process heat applications feature the requirements of different temperatures and thermal power for individual processes, when applying heat storage. Therefore, a simple storage concept needs to be adapted to satisfy the various storage requirements under different processes.

Research on many different heat exchanger concepts for latent heat storages in the temperature range between 100 °C and 250 °C have already been extensively investigated: Johnson et al. [4],[5] developed a plate heat exchanger using an eutectic mixture of KNO_3 and $NaNO_3$ as PCM. The authors examined different heat transfer structures to adapt the storage power to different applications. Saeed et al. [6] used parallel aluminium plates as heat exchanger and carried out experiments with different plate distances. Agyenim et al. [7] examined fin-and-tubes heat exchangers with the sugar alcohol erythritol as PCM. Gil et al. [8],[9] present a fin-and-tubes latent heat storage using hydrochinon as PCM. Peiró et al. [10] investigated the use of hydrochinon and D-mannitol as PCM in a fin-and-tubes heat exchanger. Steinmann et al. [11] studied a fin-and-tubes heat exchanger with graphite or aluminium fins and $NaNO_3$ or eutectic mixtures as PCM. Bayón et al. [12] further tested one of these heat exchangers in a test platform for solar thermal power plants. Zauner et al. [13] described a fin-and-tubes heat exchanger using HDPE as PCM. Shon et al. [14] presented a fin-and-tubes heat exchanger with the sugar alcohol xylitol as PCM. Wang et al. [15] investigated two shell-and-tubes heat exchangers using A 153 as PCM (melting temperature between 151 and 155 °C). They examined the heat transfer-enhancement techniques by adding homogenous and gradient metal foams. Anish et al. [16] experimentally examined a horizontal shell-and-multi-finned tube latent heat storage using erythritol as PCM and analyzed the effect of free convection during melting. Further storage concepts in the temperature range suitable for process heat applications use microcapsules and composite materials [17] or 3D-wire structures in combination with salts and their eutectic mixtures [18]. Zipf et al. [19] reported an active latent heat storage concept based on a screw heat exchanger using an eutectic mixture of $NaNO_3$ and KNO_3 as PCM. Pointner at al. [20],[21] also described an active storage concept by transporting the storage

material across the heat transfer surface. Kaizawa et al. [22] studied a direct-contact latent heat storage using the sugar alcohol erythritol as PCM. Mosleh et al. [23] tested the influence of a latent heat storage using H250, $NaNo_3$, KNO_3 and KOH as PCM in a solar power plant.

Based on the above literature review, many different heat exchanger types have been investigated, however, using of Fractherm© heat exchanger plates for latent heat storage has not been reported. As one of the novelties, this study developed and tested the heat storage using this type of heat exchanger plates. These plates have a characteristic fluid-channel design, which enables a uniform volume flow distribution and a low pressure-drop due to the flow optimization in branched fluid distribution, in comparison to standard manifold design with parallel fluid distribution [24]. The bionic FracTherm®-design was developed at Fraunhofer ISE [24] and it is the first time that it was utilized and applied to developed heat exchanger plates in PCM-storages. Due to the fabrication by roll bonding, the channels and the aluminium sheet form a union and thus lead to a good heat transfer [24]. For different storage requirements in process heat applications, different parameters such as the plate distance, the plate size and the number of channels, etc. can be adjusted, thereby providing high flexibility for the design process.

Different from the phase change temperatures higher than 200 °C where molten salts can be used, many PCMs with phase change temperatures in the range between 100 °C and 250 °C are still under research, and there is a strong demand for more materials available for this temperature range. Due to their melting ranges and high storage densities, sugar alcohols are of interest for this temperature range. Unfortunately, these materials show poor thermal stability. Thus, the studies in public domain in this sector mainly focus on the stabilization and stability enhancement of these materials [25]–[27]. For instance, some researchers tried to improve the relilablity by microencapsulation [28]. Some other materials for this temperature range are also under research, however, they present disadvantages from various aspects [29]. Accordingly, on one hand there are only a few materials available for the desired temperature range while many of them show disadvantages such as poor stability which rises a necessity of further research; on the other hand, a powerful and cost-effective heat exchanger system is also necessary to enable the efficient heat extraction or storage for industrial process applications.

FEM-simulation is a very useful and powerful tool for heat exchanger development and optimization. The influential factors which affect the heat transfer between the heat transfer fluid and the storage material on a small scale, e.g. different heat exchanger surface structures, can be well investigated using this tool. However, for larger scale simulations, e.g. optimization of heat exchanger systems or thermal energy storage systems, it has the drawback of high computation cost or long simulation durations. Therefore, a more suitable tool with high simplicity and less computation cost is of high necessity.

Descriptions and summeries on many different simplified simulation models for PCM storages can be easily found in literature [30],[31]. For instance, Pointner et al. [32] employed four different models to simulate a PCM plate storage, whose modelling results were further compared and natural convection of the PCM was considered in these numerical models. Arena et al. [33] modelled a storage using D-mannitol as PCM under three different geometrical configurations. A FEM-model was utilized in which both heat conduction and free convection were considered.

Simplified models for PCM storages were usually develooped based on resistances and capacities (RC). Mirzaei et al. [34], for instance, described a one-dimensional analytical RC-network model for PCM-storages in building applications. The model featured phase-status-dependent capacities

and resistors. Several other models for various applications can be found in literature [35] [36] [37] [38] [39]. All these publications developed RC-models, however, did not consider the decreasing of the thermal resistance due to free convection of the liquid PCM during the melting process. For applications where this effect influences the heat transfer significantly, free convection is of great importance and should be properly modelled for the sake of appropriate system sizing and design. In this study, a simplified RC-model was developed with considering free convection during the melting process in rectangular PCM gaps, based on correlations proposed by Vogel et al. [41].

Farid et al. [42] simulated a storage made of PCM-plates and using air as heat transfer fluid. In this numerical study, free convection was modelled by introducing an *effective heat conductivity* that depended on the Rayleigh-number and empirical constants related to the storage dimensions. In contrast, the RC-model developed in this study does not require any adaption of empirical constants depending on the storage dimensions.

In addition to the RC-model, a detailed physical simulation model based on the finite element method (FEM) was developed for the sake of model comparison and examination. A plate type heat exchanger with considering free convection of the liquid PCM during melting was modelled using the RC-model, which was then further verified using the FEM-model. Compared to real 3D computation, the FEM-model was significantly simplified by coupling a 2D simulation of the PCM gap between two plates with a 1D simulation for one fluid channel of the heat exchanger plate. The model was developed based on an approach proposed and validated for a fin-and- tubes heat exchanger modelling [43],[44].

Finally, the accuracy of the RC-model compared to that of the FEM-model was assessed and discussed. Both simulation models, the validation using experimental measured data, and the comparison between them are presented in the present paper.

2 Description of the system

To provide data for model validation, an experimental characterisation of the storage was carried out. The storage and the experimental setup are described in this section.

2.1 Description of the FracTherm®-plate storage

The left picture of Figure 1 shows a FracTherm®-plate used in the storage. It was made of aluminium sheet with a based thickess of 1.2 mm, and had a plane dimension of 400 mm x 150.5 mm. A series of channels were embedded within the aluminium sheet, leading to bulges with an overall thickness of 3 mm. The inlet and outlet connections to these channels were made of aluminium tubes with an outer diameter of 6 mm. Thermal oil Therminol 66® [45] was used as the heat transfer fluid, and can be drawn through the channels via the two connections.

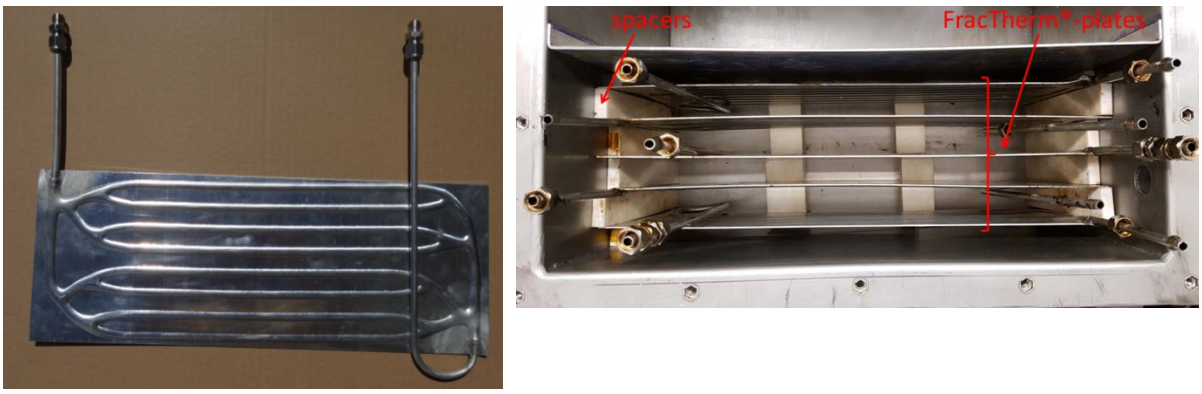

Figure 1: left: FracTherm®-plate with connection tubes; right: top view of the storage envelope including five FracTherm®-plates

The right part of Figure 1 presents a top view of the storage vessel. It consisted of a container made of stainless steel, and five FracTherm®-plates installed in parallel. These plates were installed with a distance of 25 mm by placing PTFE spacers between them at the right and the left sides. It is worthwhile to mention that the distance between the lateral plates and the container wall was a half of the distance between plates (12.5 mm). This storage vessel was able to contain the PCM with a total volume of 10.76 l, while providing a total heat transfer area of 0.6 m^2.

The connection tubes of the plates were connected in parallel using a distributor and a collector. The whole vessel was thermally insulated using rock wool with a thickness of 12 cm [46].

2.2 PCM

The sugar alcohol D-mannitol with a purity of 99.2 % was used as PCM. The relevant material properties are summarised in Table 1. 13.0 kg of D-mannitol were filled into the storage vessel in liquid state.

Table 1: Material properties of D-mannitol

Property	Value	Remark	Source
Melting temperature / °C	164.1	Onset	[47]
Melting enthalpy / kJ/kg	300.2		[47]
Density / kg/m^3	1380 (solid)/1270 (liquid)		[25]
Specific heat capacity / kJ/kgK	1.79 2.75	120 °C 180 °C	own measurement
Heat conductivity / W/mK	0.88 0.43	130 °C 190 °C	own measurement
Dynamic viscosity / Pa s	0.046	170 °C	own measurement
Volumetric coefficient of expansion / K^{-1}	1.2 10^{-4}	liquid	based on [25]

D-mannitol was selected in this study mainly due to its proper melting temperature within the temperature range of interest, even though there is a risk of degradation when heated above its

melting point [48]–[50]. Also, its high latent heat in initial state together with its high density (see Table 1) offers a high storage density. In addition, the material is non-flammable, nontoxic, non-corrosive and cost-effective [25]. Before and after the experiments, samples of the PCM were taken from the storage and the melting enthalpy was measured in DSC Q200 (from TA instruments [51]) with a heating rate of 1 K/min and a sample mass of approximately 10 mg.

Figure 2 shows a picture of the fresh D-mannitol in the storage (left) and that after the experiments (right). A clear colour change can be observed after the experiments, in which the material was remained above its melting temperature for 18 h.

Figure 2: D-mannitol in the plate heat exchanger before the measurements (left) and after the measurements (right)

Figure 3 compares the DSC-results in terms of the specific enthalpy and the specific heat capacity of the fresh D-mannitol and the post-test D-mannitol after the experiments. It can be found that the melting enthalpy decreased, and the correspoding peak became wider while merging towards a lower temperature. The melting enthalpy was 286.3 kJ/kg for the fresh D-mannitol and 237.2 kJ/kg for the post-test samples taken after experiments, resulting in a relative reduction of 17.1 %.

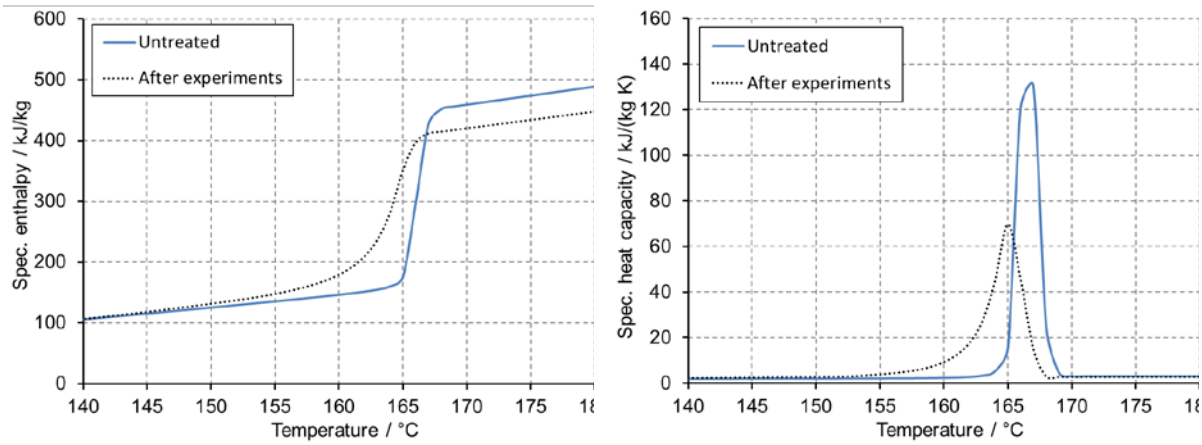

Figure 3: Comparison of the specific enthalpy (left) and the specific heat capacity (right) of untreated D-mannitol as well as the sample taken after the experiments

As a significant indicator for latent heat storage characteristation, the *Stefan number Ste* was used to quantify the ratio of sensible to latent heat capacity, which can be calculated by the following equation [41]:

$$Ste = \frac{c_p \Delta T}{h_m} \tag{1}$$

For the fresh D-mannitol and an exemplary temperature difference ΔT of 20 K, Ste reached a value of 0.19. Accordingly, the latent storage capacity was more than 5 times higher than the sensible capacity over this temperature range.

2.3 Measurement instrumentation

The storage was characterised in a test rig at Fraunhofer ISE described in [44]. The mass flow of the heat transfer fluid was measured using a Coriolis mass flow meter with an accuracy of 0.11 % at nominal flow of 0.8 kg/s [52]. The temperature sensors were calibrated Pt100-sensors with an overall accuracy of $\Delta T = \pm 0.11$ K considering the uncertainty of the reference sensor during calibration, the uncertainty of the data acquisition system and the calibration results.

The left part of Figure 4 illustrates the locations of the inlet and outlet temperature sensors and that of the mass flow sensor. The right part of Figure 4 illustrates a cross-sectional view of the plates. There were six sensors installed to measure the temperatures of PCM. Three of them were placed in the PCM at the height of 20, 75 and 130 mm between plates 2 and 3, respectively. Symmetrically, the other three temperature sensors were placed between plates 3 and 4.

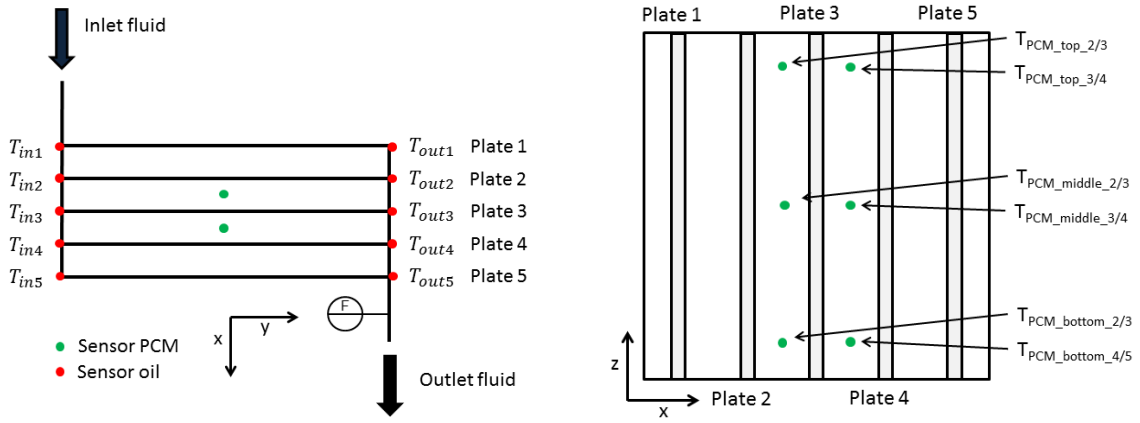

Figure 4: left: top view of the plates with positions of the temperature sensors in the thermal oil, right: cut through the plate storage in the middle of the plates in flow direction with positions of the PCM-temperature sensors

Further temperature sensors were installed at the exterior surface of the storage vessel and at the exterior surface of the thermal insulation, respectively.

2.4 Examination of free convection

The *Rayleigh-number Ra* is a commonly used measure for free convection characterisation. In terms of vertical enclosures, it can be calculated using equation (2) [53].

$$Ra = \frac{g\beta\rho^2 b^3 (T_W - T_{PCM})}{\eta^2} Pr \qquad (2)$$

The length b is the distance between the plate and the solid PCM-layer. Thus, half of the distance between two plates (i.e. 12.5 mm) is considered as this is the theoretical maximum distance between a plate and the corresponding solid PCM-layer. The left part of Figure 5 shows the Rayleigh-number as a function of the temperature difference for the maxium distance between solid PCM-layer and its corresponding heat exchanger plates. According to [53], free convection in liquids starts when Ra is higher than 2000. It corresponds to the temperature difference between the heat exchanger surface and the PCM exceeding 4 K. When the temperature difference increases over 10 K, Ra is higher than 5000. It is reported that Ra of 5000 can be regarded as a threshold, below which free convection during the melting process can be neglected in simulation models [54, S. 307]. Figure 5 right shows the Rayleigh-number over the distance b between solid PCM-layer and heat exchanger plate at a temperature difference of 10 K. Ra is higher than 2000 starting

from a distance b of 9 mm or more. At a distance of 12.5 mm or more, a value of Ra higher than 5000 can be reached. Accordingly, it indicates that the free convection can occur and should be modelled. It is expected that free convection is only developed weakly because Ra is close to the boundary values given in literature.

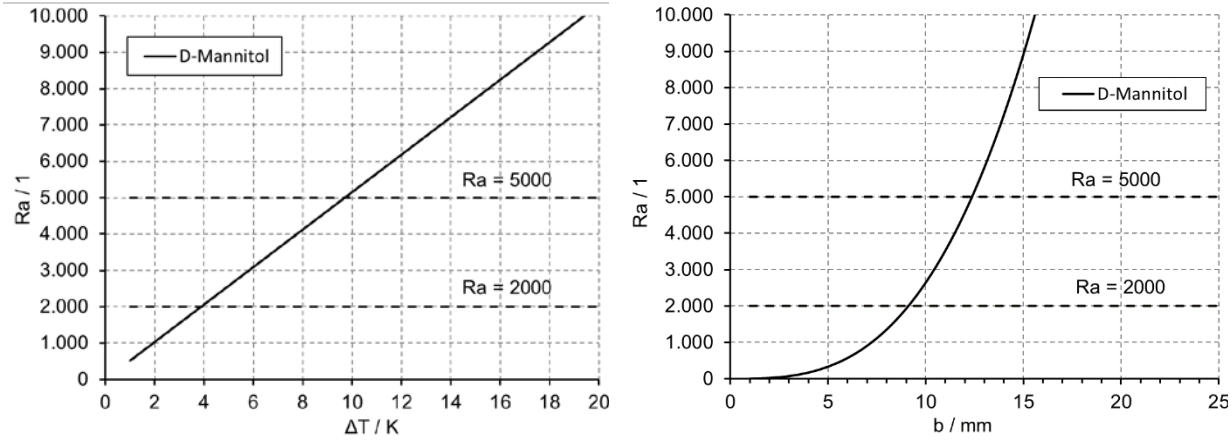

Figure 5: left: Rayleigh-number over ΔT (between plate and solid PCM-layer) at a distance of 12.5 mm, right: Rayleigh-number over the distance between plate and solid PCM-layer at a temperature difference of 10 K

3 Model description

In this section the FEM-model and the RC-models are presented and validated respectively verificated.

3.1 FEM-model

The FEM-model was developed using the software COMSOL Multiphysics® Version 5.3a [55]. Figure 6 illustrates a cross section of the plate storage, in which the small grey rectangulars represent the channels for heat transfer fluid. Due to the fact of symmetry, only the red dashed section highlighted in Figure 6 was modelled, while the total hight of the storage was considered for free convection simulation.

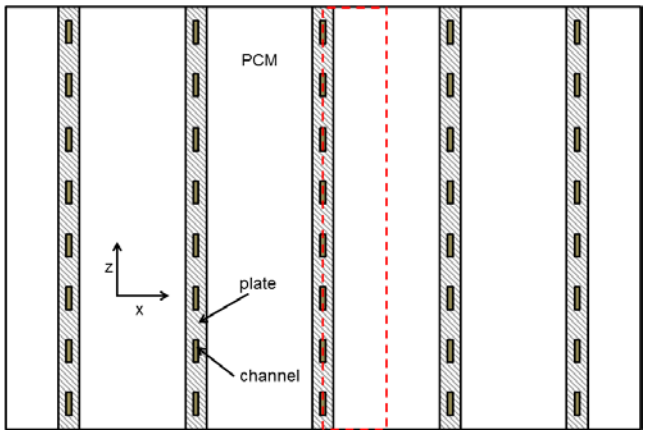

Figure 6: Cut through the plate storage in the middle of the plates in flow direction including modelling section marked in dashed red

The left picture of Figure 7 shows a 3D-drawing of a FracTherm®-plate with adjacent PCM gap (beige coloured). For the sake of simplification, the channels of the FracTherm®-plates were considered to be in parallel and the branching of the fluid channels was neglected (right side of Figure

7). The heat transfer from the plate to the PCM gap was modelled in 2D, indicated by the yellow plain in the right picture. The fluid flow in the channels in y-direction was modelled in 1D. The aforementioned two models were coupled to each other based on an approach by Wittstadt [43].

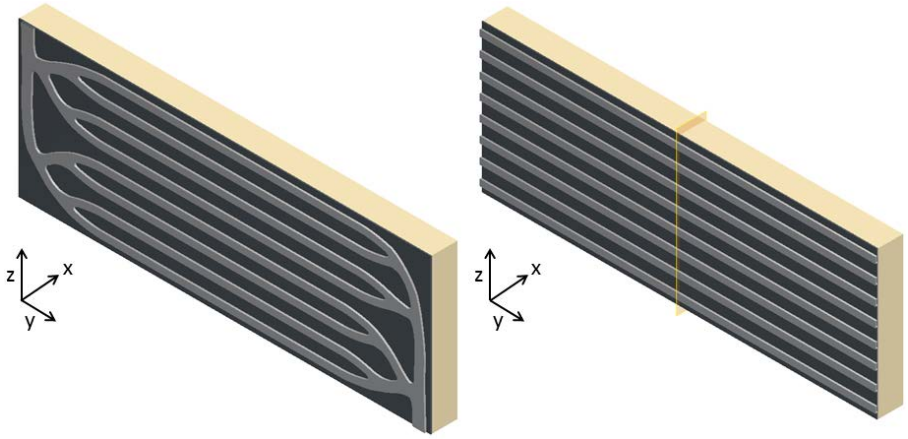

Figure 7: Left: 3D-drawing of the FracTherm®-plate with adjacent PCM gap (beige), right: alternative plate with parallel channels incl. cut (yellow) for the 2D-model

The assumptions and simplification adopted in this study were summarized as follows:

1. The heat transfer from the plate to the PCM was modelled in 2D (yellow 2D-section in Figure 7 right). Half a plate and half a PCM gap were modelled in x-direction (Figure 6).
2. The fluid channels were assumed to be stretched and in parallel (Figure 7 right). Their cross section was assumed to be rectangular [24, S. 13].
3. The temperature gradient of the fluid in radial direction of the channels was negligible. Thus, the heat transfer fluid was modelled in 1D.
4. The flow in the channels was fully developed.
5. Free convection in the liquid PCM was modelled.
    a. The flow due to free convection was regarded as laminar.
    b. The solid phase does not move, thus no sinking of the solid phase during free convection was modelled and thus no contact melting occured.
6. A volume change of the PCM during the phase change was neglected. Thus, the density was independent from the temperature. The mean value between the density in solid and liquid state was taken as simulation input parameter.
7. The other material properties of the PCM which are different in solid and liquid states were regarded as constants in solid state and in liquid state, individually.
8. The material properties of the heat transfer fluid were independent of the temperature.
9. The material properties of the heat exchanger were independent of the temperature.

3.1.1 One-dimensional model of the fluid in the rectangular channels

Figure 8 shows a sketch of the 1D-model of the fluid flow along the channels in y-direction.

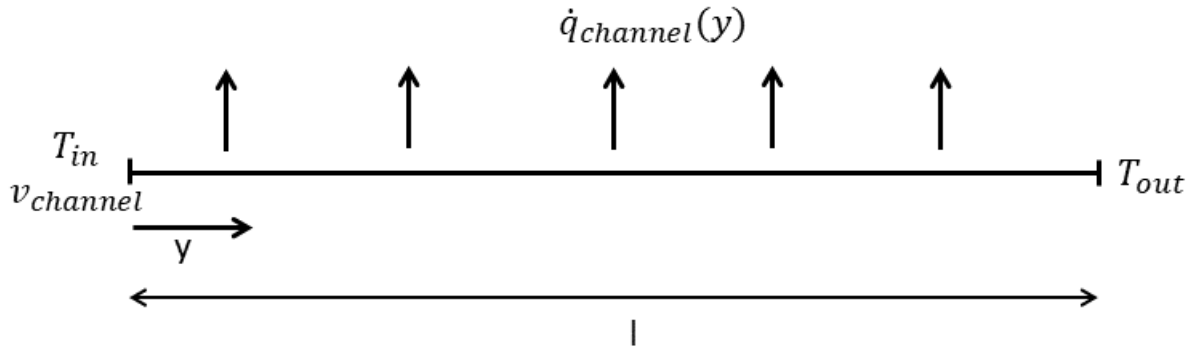

Figure 8: 1D-model of the fluid flow in the plate storage in y-direction

Only one of the eight parallel channels was modelled. This simplification is possible because the FracTherm®-channel design leads to a very even distribution of the fluid. This was also confirmed by previous infrared camera measurements which showed that the eight channels had approximately the same temperature profile. The aim of the model was to calculate the volumetric heat flux $\dot{q}_{channel}$ between the heat transfer fluid and the channel wall, as well as the outlet fluid temperature. Therefore, the temperature of the fluid in the channel can be calculated using equation (3) in COMSOL [56].

$$\rho\, c_p \frac{\partial T}{\partial t} + \rho\, c_p\, v\, \nabla T + \nabla\,(-\lambda\, \nabla T) = 0 \tag{3}$$

The following boundary conditions were implemented:

- $y = 0$: $T_{in}, v_{channel}$: The temperature and the velocity of the heat transfer fluid were implemented either as constant or as time dependent parameters at the channel inlet (Dirichlet boundary condition);
- $y = l$: $\frac{dT}{dy} = 0$: The temperature gradient at the channel outlet was zero (Neumann boundary condition); and
- y: $\dot{q}(y) = \dot{q}_{channel}$: At the whole length of the channel, a convective volumetric heat flux based on the temperature difference between the fluid and the channel wall was implemented corresponding to each node of the channel (Neumann boundary condition)

The volumetric heat flux $\dot{q}_{channel}$ between the fluid and the inner channel wall was calculated for each node according to equation (4) with the mean wall temperature T_W (explanation see chapter 3.1.3) and the local fluid temperature $T_F(y)$.

$$\dot{q}_{channel}(y) = \alpha\, \frac{A}{V}\, (T_W - T_F(y)) \tag{4}$$

The heat transfer coefficient α was calculated by a Nusselt-correlation according to [57, S. 151]. The heat transfer area A was determined using equation (5).

$$A = U_{channel}\, l \tag{5}$$

The volume V was calculated using equation (6).

$$V = b_{channel}\, d_{channel}\, l \tag{6}$$

The temperature of the inner channel wall T_W in equation (4) was calculated in the 2D-model of the plate for every time step and it was used as input value in the 1D-model.

3.1.2 Two-dimensional model with PCM and plate

Figure 9 shows a schematic drawing of the 2D-model for PCM and plate, in which the total height of the PCM gap and the plate, a half of the PCM gap, and a half of the plate are detailed. The inner channel wall is projected onto the plate area. Thus, a red line segment at y = 0 correspond to half the channel circumference. Figure 9 also details the locations of three PCM-temperatures measured corresponding to that in the experiments ($T_{PCM_{top}}$, $T_{PCM_{middle}}$, $T_{PCM_{bottom}}$), which were used for data evaluation in the following sections of this study.

The model developed was used to calculate the temperature distribution in the PCM and the plate. The simulation was carried out based on equation (3).

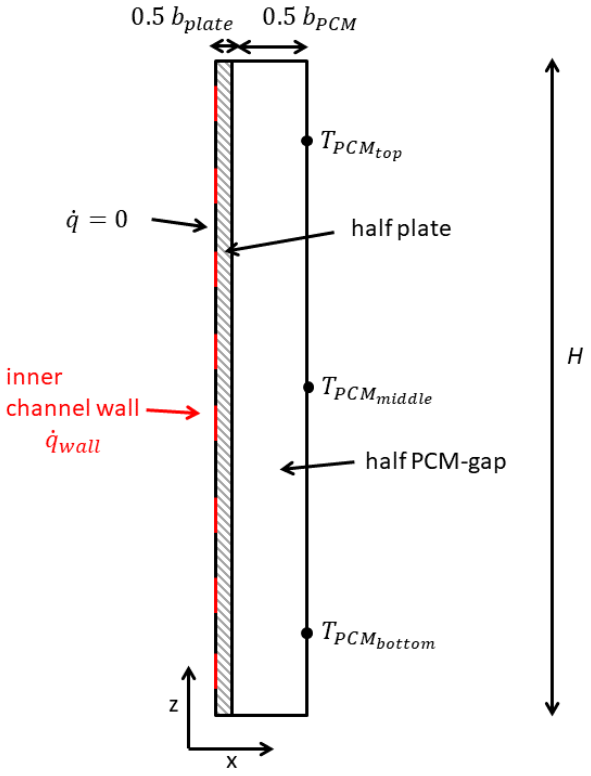

Figure 9: 2D-model of half a plate and adjacent half PCM gap with boundary conditions

If free convection of the PCM was taken into account, the flow pattern of the melted PCM was regarded as laminar flow. It was calculated according to the *momentum equation* (equation (7)) and the *continuity equation* (equation (8)) of the *Navier-Stokes-equations for incompressible fluids* [56].

$$\rho \frac{\partial v}{\partial t} + \rho (v \nabla) v = -\nabla p + \eta \Delta v + F_V \tag{7}$$

$$\rho \nabla v = 0 \tag{8}$$

The dynamic viscosity η and the volume force F_V in equation (7) can be determined using the method of the *modified viscosity* according to [58]. In this method the whole PCM is always regarded as liquid even if the temperature is below the melting temperature. In this case a *modified viscosity* forces the liquid to act as a solid by applying an extremely high viscosity. This viscosity is defined by a step function with the following properties:

$$\eta (T) = \begin{cases} 10^6, T < T_m + \Delta T/2 \\ \eta, T \geq T_m + \Delta T/2 \end{cases} \tag{9}$$

The buoyancy force leading to free convection can be defined by the volume force F_V. The *bous-sinesq-approximation* is applied. Thus, the volume force was calculated according to equation (10):

$$F_V = g\ \rho_l\ \beta\ (T - T_m) \tag{10}$$

The thermal volumetric expansion coefficient β can be calculated using a step function as described in equation (11). Accordingly, the volume force is set to 0 when the PCM is in solid state.

$$\beta = \begin{cases} 0, T < T_m + \Delta T/2 \\ \beta_l, T \geq T_m + \Delta T/2 \end{cases} \tag{11}$$

The thermal volumetric expansion coefficient β_l in liquid state of the PCM was calculated by equation (12) [59, S. 448]. Thus, a change of the density depending on the temperature in liquid state of the PCM can be considered.

$$\beta_l = -\frac{1}{\rho}\left(\frac{\partial \rho}{\partial T}\right)_p \tag{12}$$

The heat capacity of the PCM was implemented using the *capacity method* [60, S. 282]. Linearly interpolated data based on DSC-measurements were used.

The temperature dependent thermal conductivity was calculated according to equation (13) [58], in which $B(T)$ is a *smoothed heaviside function* available in COMSOL.

$$\lambda(T) = \lambda_s + (\lambda_l - \lambda_s)\ B(T) \tag{13}$$

The material properties of the aluminium heat exchanger plates were considered as constants (i.e. heat capacity $c_p = 900\ \frac{J}{kg\ K}$, thermal conductivity $\lambda = 238\ \frac{W}{m\ K}$, density $\rho = 2700\ \frac{kg}{m^3}$ [55]).

The following boundary conditions were implemented at the outer edges of the model shown in Figure 9:

- $x = 0$:
  - red line segments (i.e. inner channel walls): $\dot{q} = \dot{q}_{wall}$, calculated by the coupling of the 2D and the 1D-model;
  - Black lines (midline of the plate): adiabatic boundary condition ($\dot{q} = 0$) due to symmetry reasons;
- $x = \frac{1}{2}\left(b_{plate} + b_{PCM}\right)$: $\dot{q} = 0$, due to the fact of symmetry; and
- $z = 0$ and $z = H$: $\dot{q} = 0$, neglecting heat losses.

If free convection was considered a no-slip boundary condition, the fluid flow velocity v at the edges of the PCM gap was set as zero:

- $v = 0$

3.1.3 Coupling of the 2D- and the 1D-model

The 2D- and the 1D-models were coupled to each other by the heat flux at the inner channel wall. This means:

- The volumetric heat flux $\dot{q}_{channel}$ was calculated as an input for the 1D-model of the fluid in each time step, according to equation (4) in section 3.1.1. The mean temperature of the inner channel wall T_W, the mean temperature of the red borders in Figure 9, was calculated in the 2D-modell.
- The heat flux $\dot{q}_{wall}$ was calculated in the 2D-model as an input for each inner channel wall. It was calculated by taking a mean value over the complete channel length of the

volumetric heat flux $\dot{q}_{channel}$ achieved from the 1D-model, followed by converting it into a surface specific heat flux. As only a half of the plate was modelled, a factor if 0.5 needed to be multiplied:

$$\dot{q}_{wall} = \frac{1}{2l}\frac{V}{A}\int_0^l \dot{q}_{channel}(y)dy \tag{14}$$

3.1.4 Examination of mesh dependency

A study to determine mesh dependency was carried out. Ideally, results of a solution should be independent from the chosen number of mesh elements and time steps. In this study the aforementioned models were simulated individually to investigate the mesh dependency.

3.1.4.1 1D-model

To study the influence of the mesh for the 1D-model, a step temperature function (T_{in}) was applied at the inlet of the channel. A constant temperature (the starting temperature of the step function) was assumed at the inner channel wall T_W. Then, the simulated heat flow at the channel wall at the end of the simulation was compared to a reference case. Figure 10 shows the deviation of the heat flow in relation to the reference case with 103 degrees of freedom. The result revealed that a deviation lower than 10^{-3} can be achieved for more than 70 degrees of freedom. Thus, a mesh with 70 degrees of freedom was selected.

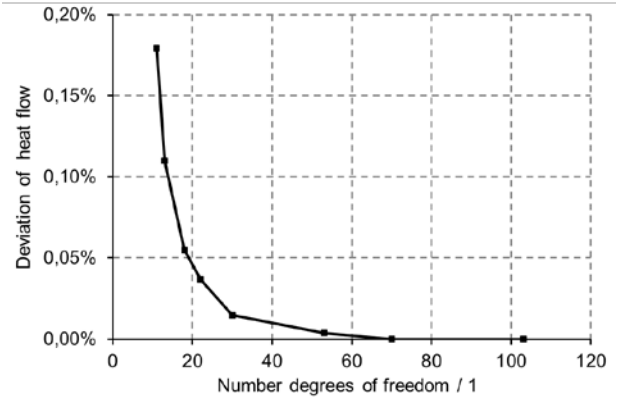

Figure 10: Deviation of the heat flow calculated in the 1D-channel compared to the reference case

3.1.4.2 2D-model

The mesh dependency of the 2D-model mainly focused on the accuracy of free convection simulation. Different from that of the 1D-model, a step temperature function was applied as the boundary condition at the channel wall. The duration of the phase change process at $T_{PCM_{middle}}$ was investigated as the key indicator to quantify the influence of mesh. Figure 11 presents the deviations between the phase change durations under different degrees of freedom compared to that of a reference case. It can be seen that neglectable phase change duration deviation can be achieved when the number of degrees of freedom reached 2.4 x 10^5 (see left part of Figure 11).

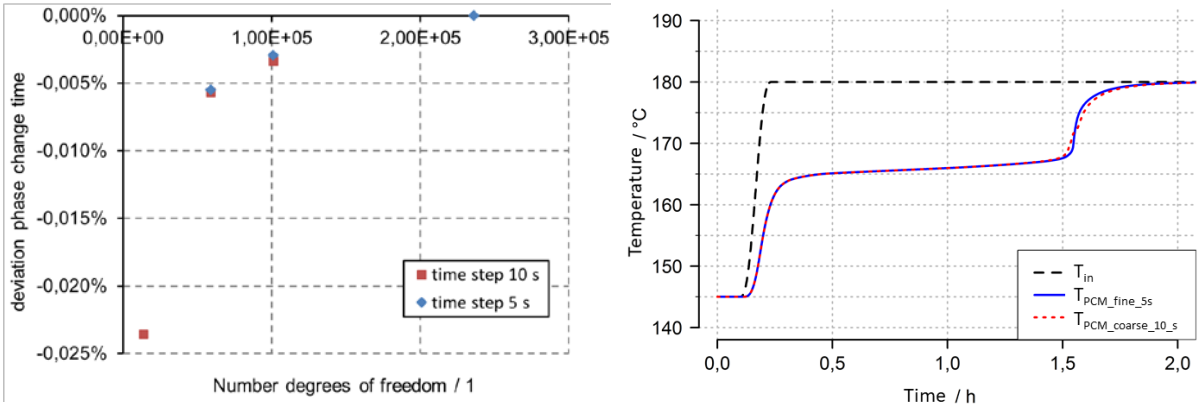

Figure 11: left: deviation of the duration of the phase change from the reference case, right: temperature for the lowest and the highest number of degrees of freedom

The start and end temperatures of the phase change are determined according to DSC-measurements. Results of the mesh dependency analysis showed that the deviations of the phase change duration were below 0.025 % in all cases. Increasing the time steps from 5 s to 10 s can be neglected. The right part of Figure 11 further shows the temperature at the position $T_{PCM_{middle}}$ for the reference simulation and the simulation with the lowest number of degrees of freedom. Basically, no clear difference can be found between the two cases. Accordingly, it is believed that a number of degrees of freedom of 13520 was enough to gain a sufficient accuracy at the location corresponding to $T_{PCM_{middle}}$.

3.1.5 Examination of free convection

The melting process of a PCM is usually dominated by thermal conduction at the beginning while by free convection at the end. Due to the fluid flow caused by free convection, the PCM on top melts faster than the PCM at the bottom. This leads to a melting front in the shape of a S-curve. [61]. This effect on the thermal behaviour of the plate storage described in section 2 was examined with the assistance of the FEM-model. Therefore, a simulative comparison with and without free convection was carried out for charging and discharging the storage. Table 1 summaries the material properties of D-mannitol used in the simulation. It is worthwhile to mention that supercooling and hysteresis between melting and solidification were neglected, and the outlet fluid temperature and the PCM-temperatures shown in Figure 9 were considered in the results.

Figure 12 shows the results for charging (left) and discharging (right). In each graph the temperature profiles for the case “with free convection” (named “conv”) are marked in black, whereas the temperature profiles of the case “without free convection” and thus based on conduction only (named “cond”) are marked in red. In both cases free convection of the PCM did not influence the outlet fluid temperature T_{out} and thus the power of the storage. During the charging process, the free convection resulted in a faster melting (around 22 min faster) of the PCM on the top of the storage, compared to that at the bottom. The temperature profile of the PCM with free convection is steeper than without free convection when leaving the phase change temperature after ca. 2.5 h. The movement of the liquid PCM in case of free convection leads to a faster rising of the temperature. The PCM on top crystallizes ca. 8 min slower than at the bottom during discharging. Additionally the phase change starts 8 min later. Accordingly, the differences among the temperatures at the three different heights are higher during the charging process than that during the discharging process, due to the different phase fronts during charging and discharging [41]. It further

verified that during discharging, natural convection can be neglected because the temperature difference was quite small, however, it must be considered during charging.

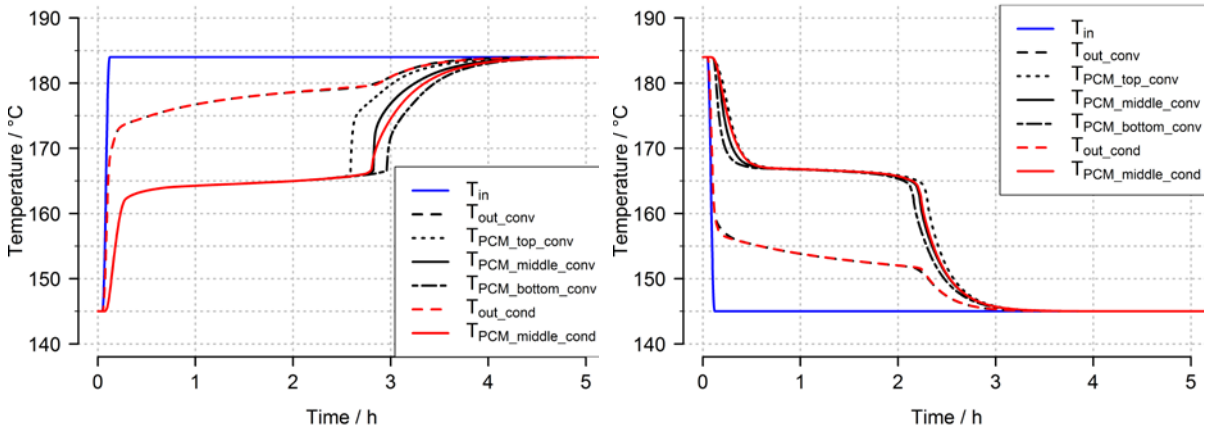

Figure 12: Simulative comparison (FEM-model) with and without free convection for the plate storage at a plate distance of 25 mm, left: charging, right: discharging

3.1.6 Model validation

Considering PCM degradation during the measurement, the c_p-curve of the post-test D-mannitol was used in the validation, as shown in Figure 3. The other material properties of D-mannitol were documented in Table 1. The Stefan number for this case was 0.23.

The mean value of the five measured inlet fluid temperatures (see Figure 4 left) was employed as inlet fluid temperature in the simulation. The outlet fluid temperature of the measurement was gained by averaging the five measured outlet fluid temperatures. The standard deviations were 1.13 K for the inlet fluid temperature and 0.69 K for the outlet fluid temperature, respectively.

During the measurement, a step increase temperature profile from 145 °C to 190 °C was controlled and implemented as the inlet temperature. The same step increase temperature profile was adopted in the numerical simulation as T_{in}. The mass flow rate of the whole storage was 1.5 kg/min and controlled constantly during the measurement, while in the simulation the corresponding constant mass flow rate was adopted. The measured and simulated oil outlet temperature as well as the measured and simulated PCM-temperatures at the three different locations (see Figure 9) were compared for the sake of model validation.

Heat losses of the storage were determined based on the measurements at static states before and after the step increasing of the inlet fluid temperature. The heat loss is calculated by equation (15).

$$\dot{Q} = \dot{m}_{oil}\, c_{p_{oil}} (T_{in} - T_{out}) \tag{15}$$

The total mass flow of 1.5 kg/min and the mean value of the five measured inlet and outlet fluid temperatures were utilised in the calculation of heat loss. It resulted in a heat loss of 66 $W \pm 64\ W$ at a temperature difference between the average exterior insulation surface and the ambient of 148 K. The high measurement uncertainty, which was calculated based on the *Gaussian error propagation,* was caused by the low temperature difference between the inlet and outlet oil temperature of less than 1 K in the static states.

In the model the full heat losses are considered to take place at the top and bottom edge of the model at $z = 0$ and $z = h$ (Figure 9).

Free convection in the liquid PCM was considered as stated in section 3.1.4.

In order to evaluate the accuracy of the simulation model, a mean deviation D between the measured and simulated temperatures was calculated according to Pointner et al. [32] using the following equation (16):

$$D = \frac{\sum_{i=0}^{i=n} |T_{sim}(t_i) - T_{meas}(t_i)|}{n+1} \quad (16)$$

where n is the number of measured points.

On the left side of Figure 13, a comparison of the temperatures between measurement and simulation is shown. Deviations between the measured and simulated outlet temperature can be observed, even though they shared a similar trend. The simulated outlet temperature strongly depended on the heat losses assumed in the model and had a relatively high measurement uncertainty. As a concequence, the simulated outlet temperature may be outside the range of the measurement uncertainty. The mean deviation between measured and simulated outlet temperature (i.e. D_{out}) until 5 hours was 1.15 K. Furthermore, the measured and simulated PCM-temperatures at the three positions given in Figure 9 were 5.65 K for $D_{PCM_{top}}$, 4.01 K for $D_{PCM_{middle}}$, and 4.18 K for $D_{PCM_{bottom}}$, respectively. To further assess these deviations, the consideration of the temperature profiles was also of necessity. It can be seen that the PCM-temperatures in measurement and simulation were in parallel until 2 hours. In both measurement and simulation, the PCM at the upper part melted faster than that at the lower part due to the fact of free convection (see section 3.1.4). There were sharp variations in the PCM-temperatures at the three measuring points from 2 hours to 3 hours, indicating the completion of phase transition at the corresponding locations. A similarly phase change process can be seen in the simulation, however, the phase transition at the three locations completed with a shorter time difference from 2.5 hours to 3 hours but the total duration of the phase change is similar.

A further sensitivity analysis showed that the heat transfer coefficient α and the locations of the temperature sensors in the PCM can influence the phase change duration by approximately ± 6 %. A measurement uncertainty of the PCM-density of ± 10 % influenced the duration of the phase change at a similar level. Measurement uncertainty of the storage losses affected the duration of the phase change up to ca. 8 %. The uncertainty of the PCM´s heat capacity and melting temperature due to its degradation additionally affected the model validation. These factors led to a high uncertainty and thus the validation via the PCM-temperatures could not be carried out more accurate.

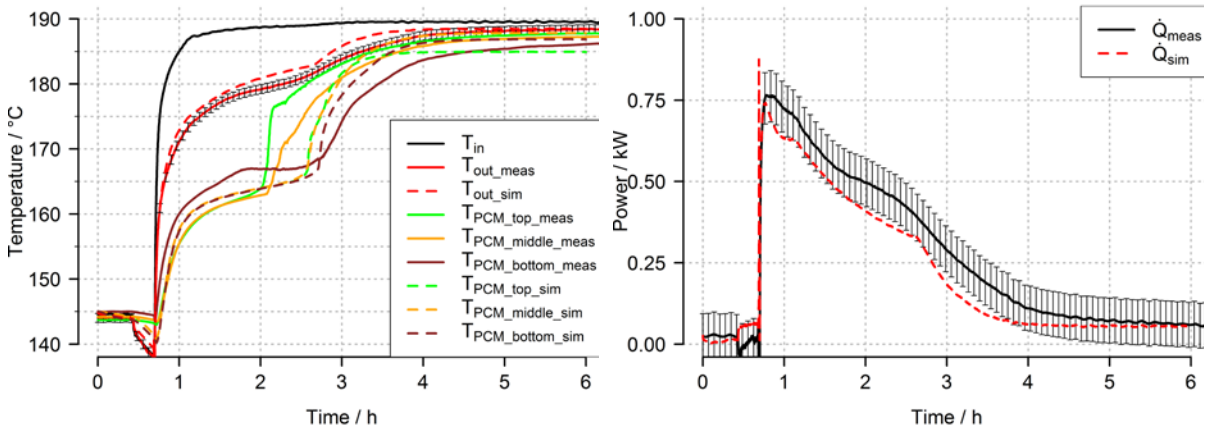

Figure 13: Validation of the FEM-model of the plate storage during charging, left: temperature profiles, right: power profile

On the right side in Figure 13, the profiles of the heat flow in measurement and simulation are shown. For both cases the heat flow was calculated according to equation (15).

The heat flow in the measurement was approximately 0.1 – 0.2 kW higher than in the simulation until 5 hours. Thus, heat release in the measurement was higher than that in the simulation. This can be explained by the described uncertainties introduced from the calculation of heat losses aforementioned. From 5.5 hours on, the heat flows in measurement and simulation were identical. Starting from this point of time the heat flow $\dot{Q}$ was only influenced by the thermal losses.

3.2 Capacitance-Resistor-Models

The RC-models were developed in the programming language Modelica® based on the Modelica® standard library version 3.2.2 [62]. Dymola Version 2017 [63] was used as modelling laboratory.

3.2.1 Modelling of the PCM

To start, an element model for the PCM gap was established. Heat transfer in the PCM is based on heat conduction or free convection, which was modelled by a thermal resistance. The storage behaviour was defined by the temperature dependent capacity of the PCM.

The PCM gap was regarded as a box-shaped element. The heat transfer was modelled in direction of the gap width. The thermal resistance in direction of the width was divided into two thermal resistances, between which the thermal capacitance was located. This symmetric element model is presented in Figure 14.

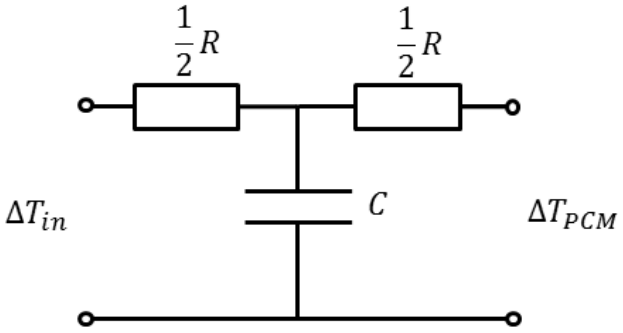

Figure 14: RC-network of the PCM gap

The temperature dependent heat capacity $C(T)$ was described by the enthalpy method [60] according to the following equation:

$$C_{PCM}(T) = \frac{m_{PCM}\, dh(T)}{dT} \tag{17}$$

The thermal resistance of the PCM was modelled in two different ways: based on heat conduction and based on free convection (and heat conduction). These models are presented as follows:

3.2.1.1 Modelling based on heat conduction

The thermal resistance R based on heat conduction across a plane wall with the width of b, height of H and thickness of d was determined according to equation (18) [64, S. 359]

$$R = \frac{b}{\lambda(T)\, H\, d} \tag{18}$$

The temperature dependent heat conductivity of D-mannitol is shown in Figure 15, considering constant values for the liquid and the solid state, individually.

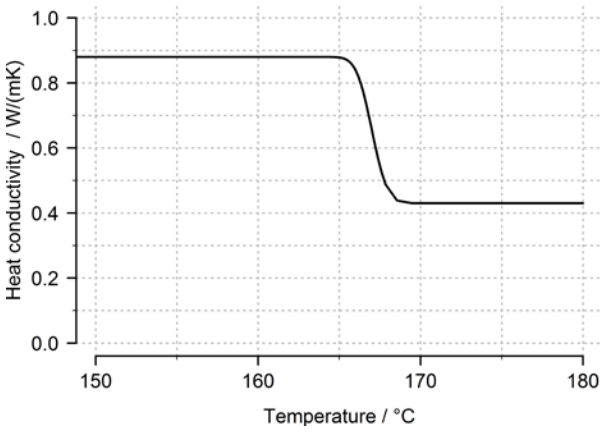

Figure 15: Temperature dependent heat conductivity of D-mannitol in the simulation

3.2.1.2 Modelling based on free convection

If free convection during the melting process of a PCM is present, a faster melting compared to a hypothetical case only based on heat conduction tends to take place. Thus, the thermal resistance of the PCM is lowered. Modelling of this lowered thermal resistance was done based on correlations developed by Vogel et al. [41]. The authors introduced a so-called mean *convective enhancement factor* $\bar{\epsilon}$. This factor was defined by the quotient of the heat flow in a case with free convection and an identical case without free convection for the same liquid fractions. Here, it was assumed that $\bar{\epsilon}$ for the proposed RC-model was not only valid for the quotient of the heat flows, but also for the quotient of the thermal resistances in the same cases.

According to Vogel et al. [41] free convection during the melting process starts at a critical liquid fraction $f_{l,crit}$, which depends on the Rayleigh-number Ra_b calculated using the width of the gap b and the ratio of its height and its width $A = \frac{H}{b}$, as described in equation (19)

$$f_{l,crit} = \sqrt[4]{\frac{150A}{Ra_b}} \tag{19}$$

The liquid fraction in the model developed in this study was calculated according to equation (20), which is the ratio of the liquid mass m_l and the total PCM-mass m_{tot}:

$$f_l = \frac{m_l}{m_{tot}} \tag{20}$$

If the liquid fraction f_l was lower than the critical liquid fraction $f_{l,crit}$ the heat transfer in the RC-model was defined by heat conduction and the thermal resistance was calculated according to equation (18). Otherwise, the thermal resistance was reduced by the factor $\bar{\epsilon}$ and was calculated according to equation (21):

$$R_{conv} = \frac{R_{cond}}{\bar{\epsilon}} \tag{21}$$

$\bar{\epsilon}$ was calculated based on the correlation given in [41]:

$$\bar{\epsilon} = \begin{cases} 1 & \text{für } Ra_b^{\frac{1}{6}} A^{-\frac{1}{4}} < 2.73 \\ 0.57 \left(Ra_b^{\frac{1}{6}} A^{-\frac{1}{4}} \right) - 0.38 & \text{für } Ra_b^{\frac{1}{6}} A^{-\frac{1}{4}} \geq 2.73 \end{cases} \tag{22}$$

3.2.1.3 Verification of the RC-models for PCM

The results obtained using the RC-models were compared to results obtained using the FEM-model described in 3.1. Only the 2D-model of a PCM gap was considered for the verification. The modelled PCM gap is shown in Figure 16.

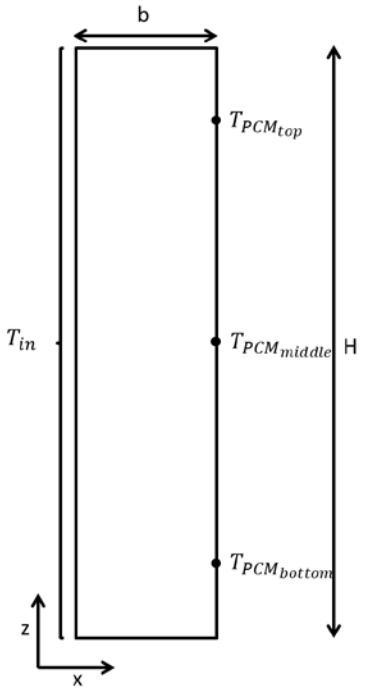

Figure 16: Sketch of the PCM gap for comparison of the RC-model to the FEM-model

A step increase temperature profile was applied to the FEM-model as input at $x = 0$. At the other three edges, the boundary condition $\dot{q} = 0$ was implemented. At the position ΔT_{in} of the RC-model (Figure 14) the same temperature step as in the FEM-model is implemented. At the position ΔT_{PCM} the boundary condition $\dot{q} = 0$ was applied. Identical dimension parameters and boundary conditions were applied in the RC-models as that utilized in the FEM-models.

In the following graphs the PCM-temperatures of the FEM-models are given at the three different heights indicated in Figure 16. However, as the RC-model cannot detail the temperature distribution over the height of the PCM, a temperature representative for a mean temperature over the height of the PCM gap is presented using the temperature T_{PCM} in the RC-model.

In all models the c_p- respectively enthalpy curve of untreated D-mannitol shown in Figure 3 and the temperature dependent heat conductivity shown in Figure 15 are adopted.

In the case based on heat conduction, the PCM-temperature over the height was constant and the melting front was vertical, thus the temperatures at the different heights have the same profile. In this case, the verification was carried out by setting the gap with both width and height of 1 cm.

The RC-model was discretised in different numbers of the elements shown in Figure 14. They were arranged in series in the direction of the gap width b. In the left picture of Figure 17, a comparison between the PCM-temperatures of the RC-model and the FEM-model is shown. It is visible that a finer discretization enabled the modelling result of the RC-model to gain a better agreement with that of the FEM-model. The mean deviations of the PCM-temperatures between the RC and the FEM-model based on equation (16) were 1.00 K for one element, 0.34 K for two elements and 0.21 K for three elements. The higher accuracy for a finer discretisation was reached because of the temperature dependent capacity and resistance. However, a discretization of more than three elements did not lead to a further relevant change of the PCM-temperature obviously. On the right side of Figure 17, the thermal resistance over time in the RC-model is shown for three elements and for one element. The thermal resistance increased with time due to the increase in temperature and the temperature dependency of the heat conductivity. When all the PCM was melted, the thermal resistance reached a maximum, because the PCM in completely liquid state had the lowest heat conductivity. If only one element was considered, the thermal resistance incresed faster, because of the absence of temperature gradient in the PCM modelling. This led to a slower melting process and a less accurate simulation.

The RC-model for the PCM based on heat conduction was regarded as verificated when at least 2 RC elements are simulated for the given gap. It is valid for other parameters, like other gap dimensions, other PCMs and other temperature steps. However, the discretisation in the direction of the gap width must be adapted depending on the dimensions and the required accuracy of the simulation model.

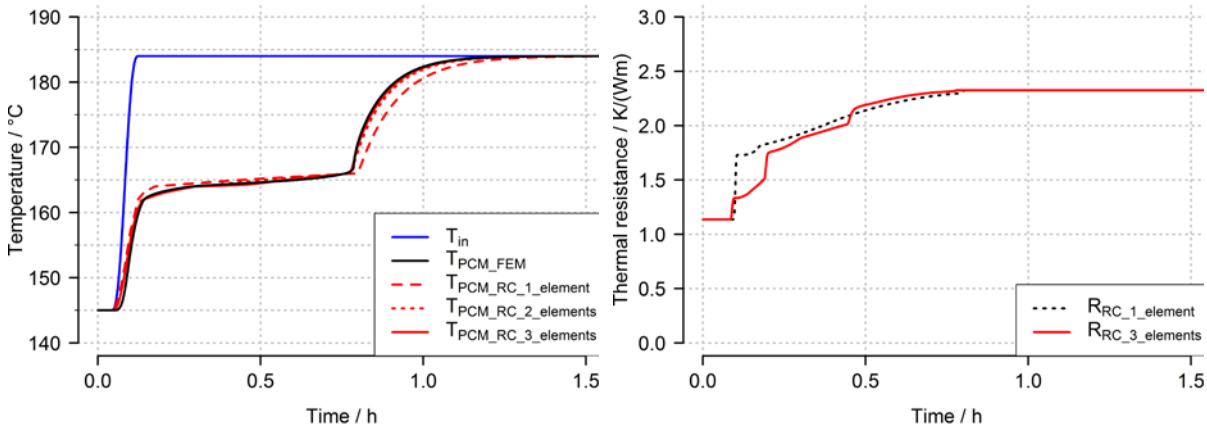

Figure 17: Comparison of the FEM-model with the RC-model of the PCM gap based on heat conduction having different element numbers: left: PCM-temperatures, right: thermal resistances

In case of the verification for the model with free convection the PCM gap in Figure 16, a width of 25 mm and a height of 150 mm were set.

Figure 18 shows a comparison between the FEM- and the RC-model based on free convection. The RC-model was divided into 20 RC-elements in x-direction because a higher number of elements does not lead to more accurate results.

Free convection in the FEM-model was considered based on the equations described in chapter 3.1.2.

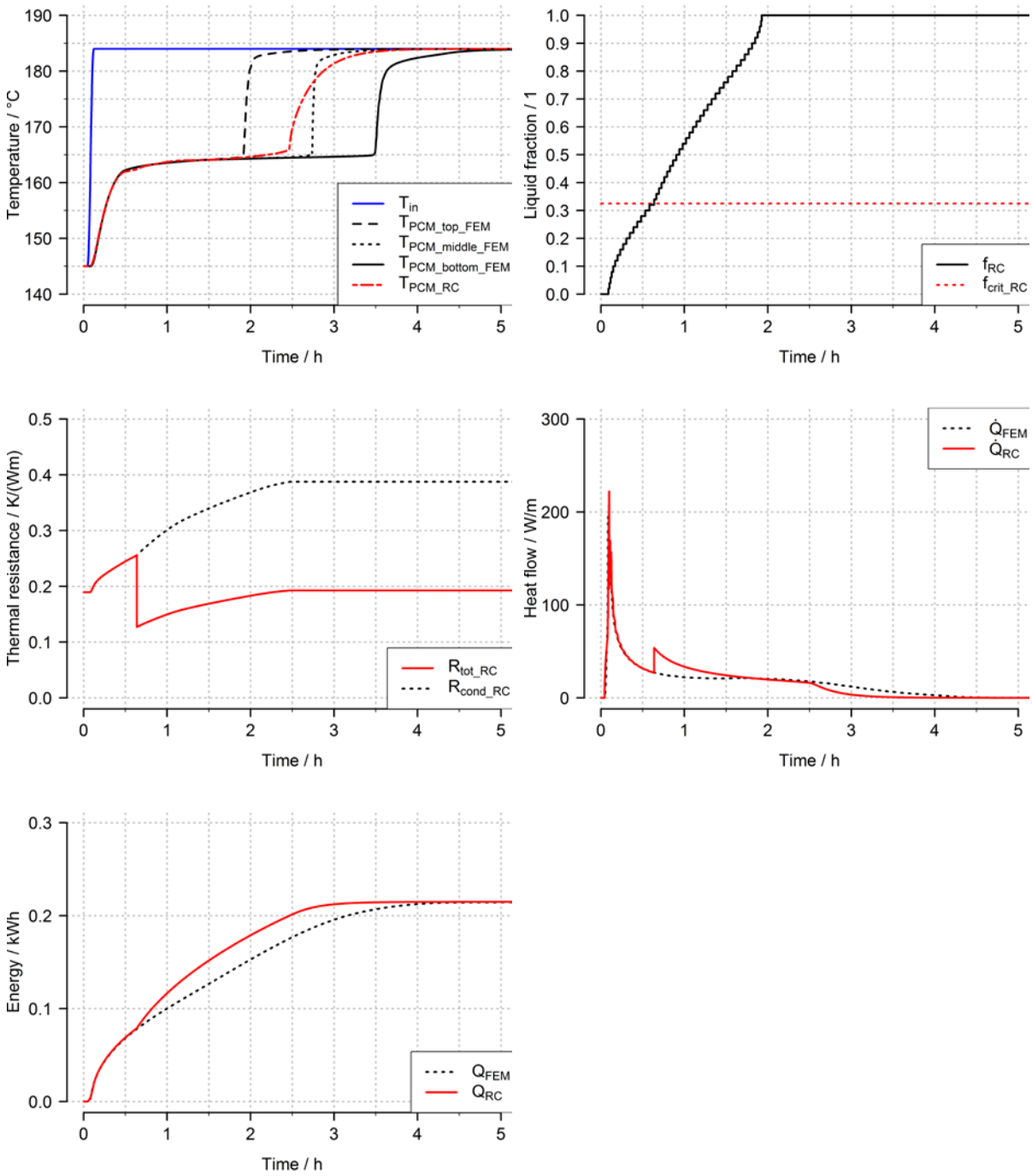

Figure 18: Comparison of the RC-network for the PCM gap based on free convection with the FEM-model having a gap width of 25 mm

In the top left figure of Figure 18, the PCM-temperatures of both models are compared to each other. In case of the FEM-model the temperature profiles at the three different heights $T_{PCM_{top}}$, $T_{PCM_{middle}}$ and $T_{PCM_{bottom}}$ indicated in Figure 16 are shown. The PCM-temperature increased after the phase change was completed, which was faster when using the FEM-model . This is due to the approach used for free convection modelling in the FEM-model (compare chapter 3.1.5). In case of the RC-model, the faster melting on top of the gap was not observed, which extended the duration of the phase transition. The mean deviation of the PCM-temperature in the RC-model to the

PCM-temperature $T_{PCM_{middle}}$ in the FEM-model ($D_{PCM_{middle}}$) calculated according to equation (16) reached 1.02 K.

In the top right graph of Figure 18, the liquid fraction as a function of time as well as the critical liquid fraction of the RC-model is shown. At the time $t = 0.6\ h$ the liquid fraction was higher than the critical liquid fraction which corresponded to the starting of the free convection.

The graph on the left side in the middle row shows the profile of the total thermal resistance in the RC-model as well as the hypothetical thermal resistance only due to heat conduction. At the beginning of the simulation, the total thermal resistance attributed to the thermal resistance based on heat conduction. Both resistances with and without considering the free convection increased until the critical liquid fraction was reached. This was due to the continuous moving of the melting front, and an increasing number of elements were melted, whose heat conductivity changed from a high value in the solid phase to a low value in the liquid phase. As soon as the critical liquid fraction was reached, the total thermal resistance was suddenly reduced by the factor $\bar{\epsilon}$ (see (21)). However, with the further moving of the melting front, the heat conductivivity experienced an increasing trend again, since the number of elements under a liquid phase with lower thermal conductivity kept increasing. After 2.5 hour, the whole PCM was fully melted and the thermal resistance reached its final value.

In the right graphic in the middle, the heat flow is presented. After the critical liquid fraction was reached at 0.6 hour, the heat flow increased abruptly due the reduction of the thermal resistance. After the fully melting of the whole PCM at 2.5 hours, the heat flow further decreased and then stablised at a relatively low value, due to decreasing of heat transfer temperature difference. It is worthwhile to mention that the transition between heat conduction and free convection in the FEM-model was smoother, and thus the start of free convection was not visible in the heat flow.

The lower left graphic shows the energy absorbed by the PCM. Due to the surge of the heat flow when free convection was triggered in the RC-model, more thermal energy was absorbed at the beginning than that of the FEM-model. Even this, at the end of the simulation the total energy stored in both models was the same.

Further verifications were carried out under different gap widths (i.e. b) of 10 mm to 40 mm with steps of 5 mm. Figure 19 shows the comparison of the PCM-temperatures for both models with the gap width of 40 mm. The PCM-temperature in the RC-model lay between the upper and lower PCM-temperature of the FEM-model. The mean deviation of the PCM-temperature in the RC-model compared to the temperature (i.e. $D_{PCM_{middle}}$) in the FEM-model was 1.54 K (calculated according to equation (3.14)). The difference in the absorbed energy between both models was 2.5 % for a gap width of 40 mm.

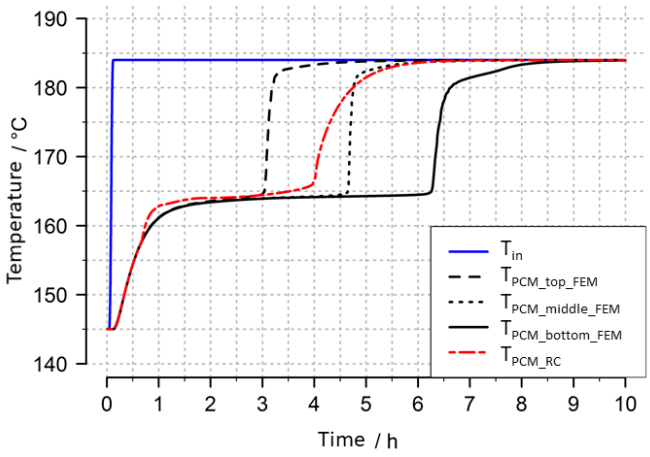

Figure 19: Comparison of the RC-network for the PCM gap based on free convection with the FEM-model having a gap width of 40 mm

These results indicate that the FEM-model outperforms the RC-model in predicting the dynamic behaviour of the PCM under the given boundary conditions with higher accurate. This is due to the different methods utilized for simulating the free convection. In the FEM-model, the development of free convection within the PCM gap was considered carefully by applying the physical equations described in section 3.1.2 for each individual element of the mesh. In specific, the whole PCM was in solid state at the beginning, whose left part started melting first when the step increase temperature was assigned to the left border (see Figure 16). The movement of the interface between molten and solid phase occurred and grew gradually towards the right part. As a consequence, the velocity of the liquid PCM started increasing slowly due to driving of the volume force. In contrast, the effect of free convection in the RC-model was actived at one defined moment when a certain layer thickness of molten PCM was reached, which deviated from the practical phenomenon.

The above discussion in terms of accuracy for the RC-model and the FEM-model under different PCM gaps with free convection is considered to be sufficient to reveal the model validity. Accordingly, the model is valid under the given boundary conditions and a maximal examined gap width of 40 mm.

Since in most applications the simulation of the whole storage is more interesting than only simulating one PCM gap, a RC-model for the whole storage including the plates is introduced in the next section.

3.2.2 Plate heat exchanger

The plate storage was modelled by a network of thermal resistances and capacitances. It coupled the above-described RC-model for the PCM, a similar RC-model for the plate, and a thermal resistance for heat transfer modelling in the liquid side. In x-direction, the same section as marked in Figure 6 was modelled, thus half a plate and half a PCM gap. In y-direction, i.e. in direction of the fluid flow, a thermal resistance for the heat transfer in the fluid was modelled. The model assumptions number 2, 4, 6, 7, 8 and 9 described in section 3.1 were considered. The RC-network is shown in Figure 20.

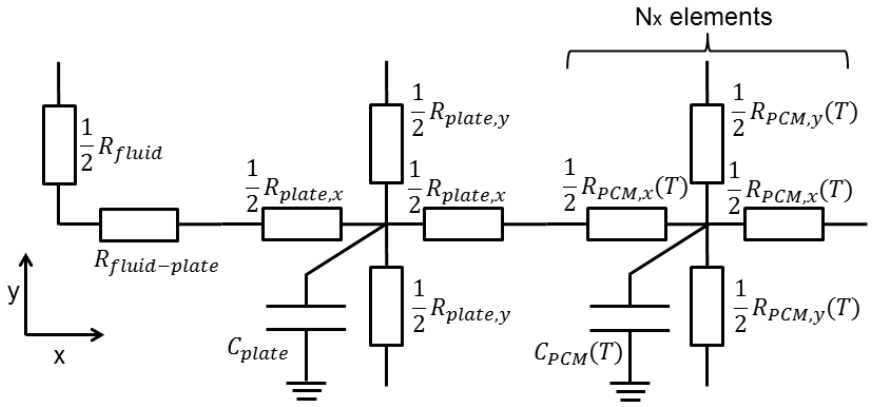

Figure 20: RC-network of a basic cell of the plate storage

On the right side the RC-model for the PCM described in chapter 3.2.1 is part of the RC-network of the plate storage. The PCM-model can be divided into an arbitrary number of elements in x-direction (i.e. in direction of the gap width), followed by a similar RC-circuit for the heat transfer in direction of the width of the plate which consisted of two resistances and a capacity. The resistances of the plate R_{plate} were calculated according to equation (18) with constant material properties. The capacity of the plate (C_{plate}) was also kept as a constant, which was calculated according to equation (23) [64, S. 71]:

$$C = m\, c_p \tag{23}$$

The thermal resistance due to the heat transfer between fluid and plate ($R_{fluid-plate}$) was calculated based on equation (24)

$$R_{fluid-plate} = \frac{1}{\alpha\, A} \tag{24}$$

The heat transfer coefficient α was calculated by a Nusselt-correlation according to [57, S. 151]. The area A is the surface area between the plate and the fluid.

The thermal resistance (R_{fluid}) was calculated according to equation (25).

$$R_{fluid} = \frac{1}{\dot{m}\, c_{p\_fluid}} \tag{25}$$

To simulate the behaviour of one total plate thereby calculating the variation of the fluid temperature in the flow direction, the RC-network was repeated by n times in flow direction. The thermal resistances of the single RC-networks were connected to each other in flow direction. Thus, the heat transfer in y-direction included by that from the fluid flow in the channel (the thermal resistance R_{fluid}) and by that from the heat conduction across the plate ($R_{plate,y}$) and the PCM ($R_{PCM,y}$).

3.2.2.1 Verification

To verificate the RC-plate model, a comparison to the FEM-model was implemented. The comparison was done for both simulations with and without free convection. In the case without free convection, the RC-model was compared to a 3D-FEM-model without free convection. The plate distance and the mass flow per plate were set as 25 mm and 0.3 kg/min, respectively. The RC-model was divided into 16 elements in the flow direction and into 8 elements in direction of the width of the PCM gap. In the case with considering free convection, a FEM-model with free convection with the 2D-1D-coupling described in sections 3.1.1 to 3.1.3 was utilized as a benchmark

for the sake of comparisoin, and the plate distance and the mass flow rate were set as 50 mm and 0.3 kg/min, respectively.

In Figure 21 the results of both comparisons are shown, in which the left side illustrates the case without free convection while the comparison cases with free convection are presented on the right side. The outlet fluid temperature and the PCM-temperature of both models had almost identical profile in the comparison when free convection was not considered. The mean deviation of the outlet fluid temperatures (D_{out}) based on equation (16) was 0.15 K and the mean deviation of the PCM-temperature (D_{PCM}) reached 0.28 K. It indicates that under the given boundary conditions, the RC-plate model without free convection can simulate the storage with a comparable accuracy to that of the 3D-FEM-model.

In the case with free convection, differences in the profile of the outlet fluid temperature and the PCM-temperature can be clearly observed. It is due to the different modelling approaches of the RC-model and the FEM-model with free convection described in section 3.2.1.3. After 2 hours, free convection started in the RC-model, thereby leading to a decrease in thermal resistance and the outlet fluid temperature. However, in the FEM-model, this transition occured smoothly and no significant variation in the outlet fluid temperature can be seen. The mean deviation between the RC- and the FEM-model (D_{out}) based on equation (16) was 0.62 K. The PCM-temperature was similar in both models until when the phase change was completed. In the RC-model, the phase change completed approximately half an hour earlier than in the FEM-model at the middle PCM position corresponding to $T_{PCM_{middle}}$. This difference was approximately 8 % of the whole phase change duration of 6 hours. The mean deviation of the PCM-temperature between the RC-model and the PCM-temperature (D_{PCM}) in the FEM-model reached 0.85 K.

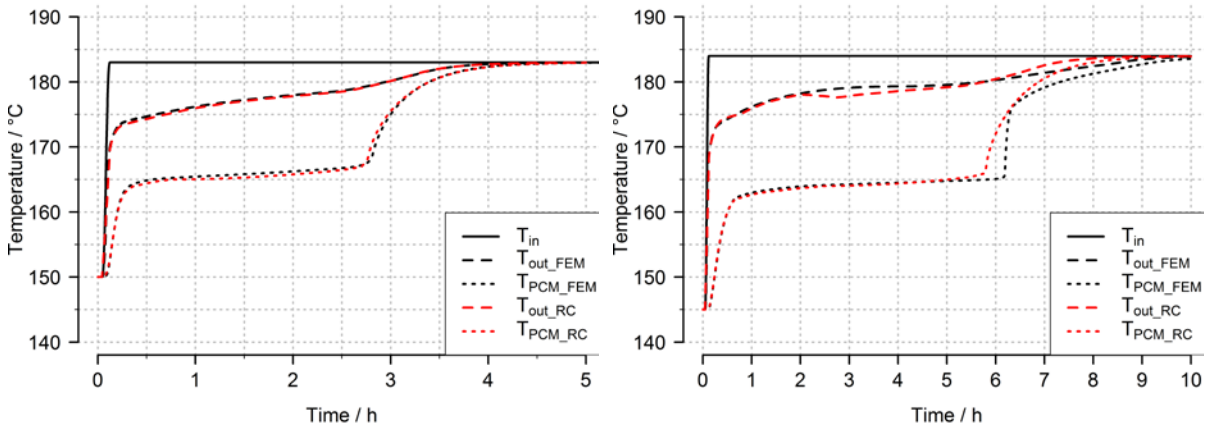

Figure 21: Comparison between the RC- and the FEM-model for the plate strorage: left: without free convection in the PCM, right: with free convection in the PCM

The results demonstrate that the accuracy of the RC-models under the present boundary conditions is high enough to be used as dimensioning tool during charging, in both cases without and with considering free convection. The model without considering free convection can be valid for other dimensions and material properties, but the discretization of the model has to be adapted in order to reach the required accuracy. In case of the model with considering free convection, the validity was carried out under the described boundary conditions and dimensions, and the given examined gap width up to 50 mm. In this case the discretization must also be adapted to reach results in the desired accuracy range. It should be examined in future, if the model with free convection is still valid for boundary conditions outside this range.

4 Conclusion and outlook

In this study a PCM storage based on FracTherm®-plates for process heat applications is presented. To the best of the authors knowledge, it is the first time that these plates were used as heat exchangers in PCM-storages. The PCM in the storage was filled between the gaps created by these plates in the PCM storage. A simplified RC-model for the storage was developed and assessed, and it was found that free convection during the melting process influences the heat transfer and must be considered in such kind model. This is a novelty which is missing in the published research from the literature. Thus, an innovative RC-model considering free convection of the PCM during the melting process in a rectangular gap was developed, validated and presented in this study. In addition, a FEM-model based on a simplified approach considering free convection was presented and validated for the sake of comparison.

The FEM-model was validated using experimental data from a lab-scale test rig. The outlet fluid temperature simulated was consistent with that of the experiment, with a mean deviation of 1.15 K. The RC-model for the rectangular PCM gap can predict the temperature at half height of the FEM-model with a maximal mean deviation of 1.54 K compared to the FEM-model. The results verify that the RC-model for the PCM gap with free convection was reliable and can be applied under the maximal examined gap width up to 40 mm. However, the RC-model including free convection is not valid for the solidification process of the PCM. A comparison of both models for the whole plate storage presented a mean deviation of the outlet fluid temperatures of 0.62 K and a mean deviation of the PCM-temperature of 0.85 K. The simulation time of the phase changing process using the RC-model was 20 to 30 times faster than that using the FEM-model.

It is believed that the RC-model developed in this study was a useful and computation-effective tool for model-based PCM storage design and optimization, while taking into account free convection of the PCM during melting. Despite its simplicity, it can still provide sufficient accuracy comparable to that of the FEM-model. The RC-model developed can also be easily adapted for the simulation of other latent heat storages where the PCM is contained in rectangular gaps and heated from one side.

It should be examined in future to see whether the model is still valid for a higher gap widths and gap height than the here examined dimensions and whether it is valid for other PCMs. In additional, it maybe valuable to further improve the RC-model by considering the free convection during the solidification process for different PCMs.

For both models presented, i.e. the simplified RC-model and the more detailed FEM-model, they can be utilized to properly size the PCM-plate-storages by determining the aceeptable parameter ranges under the given application requirements. Furthermore, a more in-depth design optimization of PCM storages can be followed and detailed using the FEM-model.

5 Acknowledgement

The authors are grateful to the German Federal Ministry for Economic Affairs and Energy for funding the work of this project (0325549A) and the Project Management Jülich for the administrative support.

References

[1] G. Hirn, F. Dr. Meyer, Latentwärmespeicher liefert Prozessdampf, 09/08.

[2] M. Sterner, I. Stadler, Energiespeicher - Bedarf, Technologien, Integration, Springer Berlin, Berlin, 2014.

[3] A. Hauer, S. Hiebler, M. Reuss, Wärmespeicher, 5th ed., Fraunhofer IRB Verlag, Stuttgart, 2013.

[4] M. Johnson, M. Fiß, T. Klemm, Experimental Testing of Various Heat Transfer Structures in a Flat Plate Thermal Energy Storage Unit, in: SolarPACES: Concentrating Solar Power and Chemical Energy Sytems, 2015.

[5] M. Johnson, M. Fiss, T. Klemm, M. Eck, Test and Analysis of a Flat Plate Latent Heat Storage Design, Energy Procedia 57 (2014) 662–671.

[6] R.M. Saeed, J.P. Schlegel, R. Sawafta, V. Kalra, Plate type heat exchanger for thermal energy storage and load shifting using phase change material, Energy Conversion and Management 181 (2019) 120–132.

[7] F. Agyenim, P. Eames, M. Smyth, A comparison of heat transfer enhancement in a medium temperature thermal energy storage heat exchanger using fins, Solar Energy 83 (2009) 1509–1520.

[8] A. Gil, E. Oró, A. Castell, L.F. Cabeza, Experimental analysis of the effectiveness of a high temperature thermal storage tank for solar cooling applications, Applied Thermal Engineering 54 (2013) 521–527.

[9] A. Gil, E. Oró, L. Miró, G. Peiró, Á. Ruiz, J.M. Salmerón, L.F. Cabeza, Experimental analysis of hydroquinone used as phase change material (PCM) to be applied in solar cooling refrigeration, International Journal of Refrigeration 39 (2014) 95–103.

[10] Gerard Peiró, Jaume Gasia, Laia Miró, Luisa F. Cabeza, Experimental evaluation at pilot plant scale of multiple PCMs (cascaded) vs. single PCM configuration for thermal energy storage, Renewable Energy 83 (2015) 729–736.

[11] W.-D. Steinmann, D. Laing, R. Tamme, Development of PCM Storage for Process Heat and Power Generation 131 (2009) 410091–410094.

[12] R. Bayón, E. Rojas, L. Valenzuela, E. Zarza, J. León, Analysis of the experimental behaviour of a 100 kWth latent heat storage system for direct steam generation in solar thermal power plants, Applied Thermal Engineering 30 (2010) 2643–2651.

[13] C. Zauner, F. Hengstberger, M. Etzel, D. Lager, R. Hofmann, H. Walter, Experimental characterization and simulation of a fin-tube latent heat storage using high density polyethylene as PCM, Applied Energy 179 (2016) 237–246.

[14] J. Shon, H. Kim, K. Lee, Improved heat storage rate for an automobile coolant waste heat recovery system using phase-change material in a fin–tube heat exchanger, Applied Energy 113 (2014) 680–689.

[15] Z. Wang, J. Wu, D. Lei, H. Liu, J. Li, Z. Wu, Experimental study on latent thermal energy storage system with gradient porosity copper foam for mid-temperature solar energy application, Appl. Energ. 261 (2020) 114472.

[16] R. Anish, V. Mariappan, M. Mastani Joybari, Experimental investigation on the melting and solidification behavior of erythritol in a horizontal shell and multi-finned tube latent heat storage unit, Applied Thermal Engineering 161 (2019) 114194.

[17] W.-D. Steinmann, R. Tamme, Latent Heat Storage for Solar Steam Systems, Journal of Solar Energy Engineering 130 (2007) 011004-011004-5.

[18] A. Schlott, J. Hörstmann, O. Andersen, J. Meinert, High Power Latent Heat Storages with 3D Wire Structures – Numerical Evaluation of Phase Change Behavior, in: EUROSOLAR- Europäische Vereinigung für Erneuerbare Energien e.V. (Ed.), 11th International Renewable Energy Storage Conference (IRES 2017), 2017.
[19] V. Zipf, A. Neuhäuser, D. Willert, P. Nitz, S. Gschwander, W. Platzer, High temperature latent heat storage with a screw heat exchanger: Design of prototype, Appl. Energ. 109 (2013) 462–469.
[20] H. Pointner, W.-D. Steinmann, Experimental demonstration of an active latent heat storage concept, Applied Energy 168 (2016) 661–671.
[21] H. Pointner, W.-D. Steinmann, M. Eck, Introduction of the PCM Flux Concept for Latent Heat Storage, 6th International Building Physics Conference, IBPC 2015 57 (2014) 643–652.
[22] A. Kaizawa, H. Kamano, A. Kawai, T. Jozuka, T. Senda, N. Maruoka, T. Akiyama, Thermal and flow behaviors in heat transportation container using phase change material, Energy Conversion and Management 49 (2008) 698–706.
[23] H. Jafari Mosleh, R. Ahmadi, Linear parabolic trough solar power plant assisted with latent thermal energy storage system: A dynamic simulation, Applied Thermal Engineering 161 (2019) 114204.
[24] M. Hermann, Bionische Ansätze zur Entwicklung energieeffizienter Fluidsysteme für den Wärmetransport. Dissertation, Karlsruhe, 2005.
[25] E. Palomo del Barrio, A. Godin, M. Duquesne, J. Daranlot, J. Jolly, W. Alshaer, T. Kouadio, A. Sommier, Characterization of different sugar alcohols as phase change materials for thermal energy storage applications, Solar Energy Materials and Solar Cells 159 (2017) 560–569.
[26] H. Neumann, D. Burger, Y. Taftanazi, M.P. Alferez Luna, T. Haussmann, G. Hagelstein, S. Gschwander, Thermal stability enhancement of d-mannitol for latent heat storage applications, Solar Energy Materials and Solar Cells 200 (2019) 109913.
[27] S.N. Gunasekara, R. Pan, J.N. Chiu, V. Martin, Polyols as phase change materials for surplus thermal energy storage, Appl. Energ. 162 (2016) 1439–1452.
[28] L. He, S. Mo, P. Lin, L. Jia, Y. Chen, Z. Cheng, D-mannitol@silica/graphene oxide nanoencapsulated phase change material with high phase change properties and thermal reliability, Appl. Energ. 268 (2020) 115020.
[29] D. Haillot, T. Bauer, U. Kröner, R. Tamme, Thermal analysis of phase change materials in the temperature range 120 to 150 °C, Thermochimica Acta 513 (2011) 49–59.
[30] Yvan Dutil, Daniel R. Rousse, Nizar Ben Salah, Stéphane Lassue, Laurent Zalewski, A review on phase-change materials: Mathematical modeling and simulations, Renewable and Sustainable Energy Reviews 15 (2011) 112–130.
[31] Abduljalil A. Al-abidi, Sohif Bin Mat, K. Sopian, M.Y. Sulaiman, Abdulrahman Th. Mohammed, CFD applications for latent heat thermal energy storage: a review, Renewable and Sustainable Energy Reviews 20 (2013) 353–363.
[32] H. Pointner, A. de Gracia, J. Vogel, N.H.S. Tay, M. Liu, M. Johnson, L.F. Cabeza, Computational efficiency in numerical modeling of high temperature latent heat storage: Comparison of selected software tools based on experimental data, Applied Energy 161 (2016) 337–348.
[33] S. Arena, G. Cau, C. Palomba, CFD Simulation of Melting and Solidification of PCM in Thermal Energy Storage Systems of Different Geometry, Journal of Physics: Conference Series 655 (2015) 12051.
[34] P.A. Mirzaei, F. Haghighat, Modeling of phase change materials for applications in whole building simulation, Renewable and Sustainable Energy Reviews 16 (2012) 5355–5362.

[35] A. Stupar, U. Drofenik, J. Kolar, Application of Phase Change Materials for Low Duty Cycle High Peak Load Power Supplies, in: 6th International Conference on Integrated Power Electronics Systems: CIPS 2010, 2010.
[36] A. Tilli, A. Bartolini, M. Cacciari, L. Benini, Don't burn your mobile!, in: A. Jerraya (Ed.), Proceedings of the eighth IEEEACMIFIP international conference on Hardwaresoftware codesign and system synthesis, ACM, New York, NY, 2012, p. 373.
[37] J. Gao, T. Yan, T. Xu, Z. Ling, G. Wei, X. Xu, Development and experiment validation of variable-resistance-variable-capacitance dynamic simplified thermal models for shape-stabilized phase change material slab, Applied Thermal Engineering 146 (2019) 364–375.
[38] A. Bontemps, M. Ahmad, K. Johannès, H. Sallée, Experimental and modelling study of twin cells with latent heat storage walls, Energy and Buildings 43 (2011) 2456–2461.
[39] N. Zhu, S. Wang, X. Xu, Z. Ma, A simplified dynamic model of building structures integrated with shaped-stabilized phase change materials, International Journal of Thermal Sciences 49 (2010) 1722–1731.
[40] H. Behi, M. Ghanbarpour, M. Behi, Investigation of PCM-assisted heat pipe for electronic cooling, Applied Thermal Engineering 127 (2017) 1132–1142.
[41] J. Vogel, J. Felbinger, M. Johnson, Natural convection in high temperature flat plate latent heat thermal energy storage systems, Applied Energy 184 (2016) 184–196.
[42] M.M. Farid, R.M. Husian, An electrical storage heater using the phase-change method of heat storage, Energ Convers Manage (1990) 219–230.
[43] U. Wittstadt, Experimentelle und modellgestützte Charakterisierung von Adsorptionswärmeübertragern. Dissertation, Berlin, 2018.
[44] H. Neumann, V. Palomba, A. Frazzica, D. Seiler, U. Wittstadt, S. Gschwander, G. Restuccia, A simplified approach for modelling latent heat storages: Application and validation on two different fin-and-tubes heat exchangers, Applied Thermal Engineering 125 (2017) 41–52.
[45] FRAGOL AG, Therminol 66 Datenblatt, https://www.fragol.de/?id=210&file=30004dRk_Therminol_66_Produktinformation.pdf&L=0, accessed 17 August 2015.
[46] Paroc Group, Paroc Pro Slab 80: Datenblatt, http://www.paroc.de/losungen-und-produkte/produkte/pages/dammplatten-fur-industielle-anwendungenden-miterhohter-warmeeinwirkung/paroc-pro-slab-80, accessed 15 February 2017.
[47] B. Tong, R.-B. Liu, C.-G. Meng, F.-Y. Yu, S.-H. Ji, Z.-C. Tan, Heat Capacities and Nonisothermal Thermal Decomposition Reaction Kinetics of d-Mannitol, Journal of Chemical & Engineering Data 55 (2010) 119–124.
[48] H. Neumann, S. Niedermaier, S. Gschwander, P. Schossig, Cycling stability of d-mannitol when used as phase change material for thermal storage applications, Thermochimica Acta 660 (2018) 134–143.
[49] A. Solé, H. Neumann, S. Niedermaier, I. Martorell, P. Schossig, L.F. Cabeza, Stability of sugar alcohols as PCM for thermal energy storage, Solar Energy Materials and Solar Cells 126 (2014) 125–134.
[50] R. Bayón, E. Rojas, Feasibility study of d-mannitol as phase change material for thermal storage, AIMS Energy 5 (2017) 404–424.
[51] TA Instruments, DSC Q200, https://www.tainstruments.com/, accessed 19.11.19.
[52] Rota Yokogawa GmbH & Co. KG, Produkt Spezifikation GS 01R04B04-00D-E: ROTAMASS 3 Serie Coriolis Massedurchfluss- und Dichtemesser, 2017,

https://www.yokogawa.com/de/fld/durchfluss/coriolis/de_dokumente/new/GS01R04B04-00D-E_25.pdf, accessed 26.3.19.
[53] Deborah A. Kaminski, Michael K. Jensen, Convection Heat Transfer: Chapter 12, in: Deborah A. Kaminski, Michael K. Jensen (Ed.), Introduction to Thermal and Fluids Engineering, Updated Edition, 2011.
[54] I. Dincer, M. Rosen, Thermal Energy Storage: Systems and Applications, John Wiley & Sons, 2002.
[55] COMSOL INC., COMSOL MULTIPHYSICS(R).
[56] COMSOL Multiphysics 5.3a User Guide.
[57] H. Recknagel, E. Sprenger (Eds.), Taschenbuch für Heizung und Klimatechnik, DIV, Dt. Industrieverl., München, 2007.
[58] F. Samara, D. Groulx, P.H. Biwole, Natural Convection Driven Melting of Phase Change Material: Comparison of Two Methods, in: COMSOL Conference Boston, 2012.
[59] H.D. Baehr, K. Stephan, Wärme- und Stoffübertragung, 6th ed., Springer-Verlag Berlin Heidelberg, 2008.
[60] P. Lamberg, R. Lehtiniemi, A.-M. Henell, Numerical and experimental investigation of melting and freezing processes in phase change material storage, International Journal of Thermal Sciences 43 (2004) 277–287.
[61] J. Vogel, D. Bauer, Phase state and velocity measurements with high temporal and spatial resolution during melting of n-octadecane in a rectangular enclosure with two heated vertical sides, International Journal of Heat and Mass Transfer 127 (2018) 1264–1276.
[62] ABB, AIT, T. Bödrich, DLR, Dassault Systèmes AB, Fraunhofer, A. Haumer, ITI, C. Kral, Modelon, TU, Modelica Standard Library, Modelica Association, 1998-2016.
[63] Dymola: Dynamic Modeling Laboratory, Dassault Systèmes, 2016.
[64] G. Cerbe, G. Wilhelms, Technische Thermodynamik: Theoretische Grundlagen und praktische Anwendungen ; mit 38 Tafeln, 129 Beispielen, 137 Aufgaben und 181 Kontrollfragen, 14th ed., Hanser, München [u.a.], 2007.